ISSN 0957-4484

NANOTECHNOLOGY

VOLUME 19 NUMBER 20 21 MAY 2008

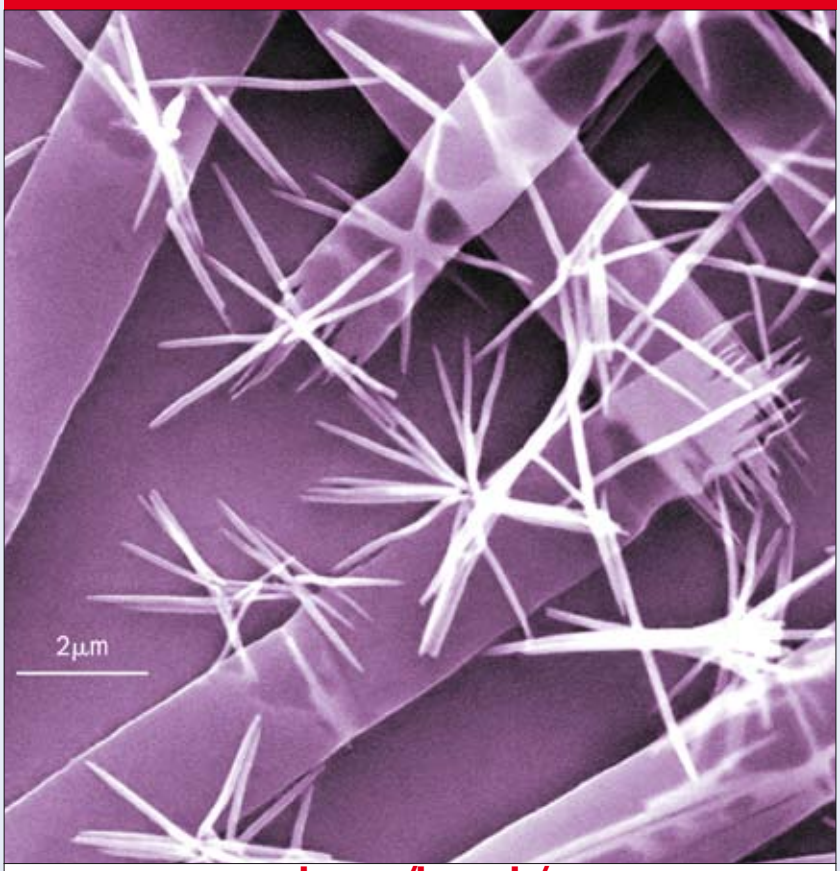

www.iop.org/journals/nano

Featured article

Continuous-flow laser synthesis of large quantities of iron oxide nanowires in solution

S Mollah, S J Henley and S R P Silva

IOP Publishing

Nanotechnology **19** (2008) 205709 (10pp) doi:10.1088/0957-4484/19/20/205709

Interactions between halloysite nanotubes and 2,5-bis(2-benzoxazolyl) thiophene and their effects on reinforcement of polypropylene/halloysite nanocomposites

Mingxian Liu, Baochun Guo[1], Quanliang Zou, Mingliang Du and Demin Jia

Department of Polymer Materials and Engineering, South China University of Technology, Guangzhou 510640, People's Republic of China

E-mail: psbcguo@scut.edu.cn

Received 17 January 2008, in final form 12 March 2008
Published 15 April 2008
Online at stacks.iop.org/Nano/19/205709

Abstract

Many types of clay tend to absorb organics via electron transferring interactions between the clay and the organics. This may be utilized to design clay incorporated polymer composites with better interfacial properties. In the present paper, 2,5-bis(2-benzoxazolyl) thiophene (BBT), capable of donating electrons, is selected as the interfacial modifier for polypropylene (PP)/halloysite nanotube (HNTs) composites. The electron transfer between HNTs and BBT are confirmed. The mechanical properties and the unique morphology of the nanocomposites are examined. Formation of fibrils of BBT in the presence of HNTs is found in the nanocomposites. The chemical composition of the fibrils in the nanocomposites is found to be composed of largely BBT and a small amount of HNTs. The formation mechanism of BBT fibrils are elucidated to be the strong interactions between BBT and HNTs under melt shearing. The formation of the BBT fibrils leads to much higher crystallinity compared with previously reported PP nanocomposites. The nanocomposites with BBT show substantially increased tensile and flexural properties, which are attributed to the enhanced crystallinity of the nanocomposites.

(Some figures in this article are in colour only in the electronic version)

1. Introduction

Polymer nanocomposites incorporating nanosized particles have attracted a great deal of attention due to their unique structures and unusual properties which could not be achieved by conventional composites [1, 2]. Numerous strategies for improving the interfacial bonding and overall performance of the polymer nanocomposites have been reported. The sol–gel process constitutes a primary *in situ* dispersion method of nanoparticles with precursors [3]. Compared with *in situ* formation of nanoparticles, pretreatment of nanoparticles is more common in the fabrication of nanocomposites. Surface initiated polymerization (SIP) is one class of effective method for the treatment of nanoparticles before their incorporation into the polymers [4, 5]. In comparison with SIP methods, addition of modifiers such as coupling agents [6, 7], surfactants [8, 9], grafts [10, 11], etc, is much more convenient and easier to scale up. The interaction mechanisms between the modifier and nanoparticle including van der Waals force, covalent bonding, hydrogen bonding, ionic bonding or physical entanglements have been widely reported.

Halloysite nanotubes (HNTs) offer great opportunities for fabricating polymer nanocomposites with promising performance [12–15]. HNTs, chemically similar to kaolinite with a molecular formula of $Al_2Si_2O_5(OH)_4 \cdot nH_2O$, are multi-walled inorganic nanotubes. The tubular halloysite is formed by rolling of a kaolin sheet in preference to tetrahedral rotation to correct the misfit of the octahedral and tetrahedral

[1] Author to whom any correspondence should be addressed.

sheets [16]. Comparing with carbon nanotubes (CNTs), the naturally occurred HNTs are much cheaper and easily available. An ideal HNT crystal consists of a nonexpansive, layered structure that contains octahedrally coordinated Al^{3+} and tetrahedrally coordinated Si^{4+} in a 1:1 stoichiometric ratio [17]. Different from most clays, most aluminols are located in the inner of the HNTs, while in the outer of the HNTs are primarily siloxane and a few silanols and aluminols which are exposed in the edges of the sheet. The relatively low content of hydroxyl groups on the surface of HNTs leads to limited reactive sites for covalent bonding. Consequently, the chemical modification of HNTs by the above-mentioned methods is not usually satisfactory [18]. Fortunately, the presence of several metal atoms on HNTs, such as aluminum, iron and transition metals with unoccupied orbitals [19], offers great opportunities for improving the interfacial properties between HNTs and polymers or organics via electron transfer interactions. Actually many clays capable of absorbing organics via an electron transfer mechanism have been reported [20–23]. Solomon *et al* reported the polymerization of monomers on clay surfaces through an electron transferring mechanism and found that the kaolinite and montmorillonite could catalyze the polymerization of monomers such as styrene and hydroxyethyl methacrylate [24]. Organic interlamellar complexes of HNTs have also been studied. Carr and Chih reported the interactions of various organic complexes of halloysite with polar organic compounds [25]. The general review by Theng summarized most of the significant work on the preparation of organic complexes of HNTs [26].

For better interfacial properties, electron transfer interactions were introduced into HNTs incorporated polypropylene (PP) nanocomposites in the present work. A common fluorescent brightener, 2,5-bis(2-benzoxazolyl) thiophene (BBT), capable of donating electrons [27, 28] was selected as the interfacial modifier for PP/HNTs systems. The interactions between HNTs and BBT were studied. The mechanical properties and the unique morphology of the nanocomposites were examined. The relationships of HNTs/BBT interactions, the morphology and consequent reinforcing effects of the nanocomposites were suggested. Although the surface chemistry and geometry of CNTs are quite different from those of HNTs, in our opinion, the idea of designing an interface via charge transfer, may also be applicable to CNTs incorporating polymer composites.

2. Experimental details

2.1. Materials

The isotactic PP, with a melt flow index of 2.84 g/10 min (after ISO-1133: 1997(E)), was purchased from Lanzhou Petro-chemical Co., China. The HNTs, mined from Yichang, Hubei, China, were purified according to [29]. A typical procedure is described below. A 10 wt% water solution of halloysite was prepared by slow addition of water to dry halloysite. Then 0.05 wt% sodium hexametaphosphate was added to the solution while stirring. The solution was stirred for 30 min and left to stand for 20 min at room temperature. The clay aggregate and impurities were precipitated in the bottom and were removed by filtration. The upper solution was carefully collected and the resulting HNTs were separated by centrifugation and dried at 80 °C in air for 5 h. The elemental composition of purified HNTs by x-ray fluorescence (XRF) was determined as follows (wt%): SiO_2, 58.91; Al_2O_3, 40.41; Fe_2O_3, 0.275; TiO_2, 0.071. BBT with a melting point of 219 °C was purchased from Guangzhou Times Chemical Factory, China and used as received. The chemical structure of the BBT is depicted below.

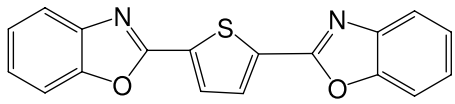

2.2. Characterization of interaction between HNTs and BBT

2.2.1. Surface area and pore structure analysis. The HNTs/BBT complex was prepared by blending HNTs and BBT vigorously. The Brunauer–Emmett–Teller (BET) surface area and pore structure of HNTs and the HNTs/BBT complex were investigated using the nitrogen adsorption method with Micromeritics ASAP 2020. Prior to the determination of an adsorption–desorption isotherm the sample was degassed to remove the physisorbed species from the surface of HNTs. The sample was degassed to 0.2 mm Hg with an evacuation rate 5 mm Hg s^{-1} and a heating procedure with a heating ratio 10 °C min^{-1} to 90 °C. Then the sample was heated to 200 °C with a heating ratio 10 °C min^{-1} and held at 200 °C for 3 h. The specific surface area was calculated by applying the BET method to the relative pressure (P/P^0) range of the isotherms between 0.05 and 0.2, taking a value of 0.162 nm^2 for the cross section of the adsorbed nitrogen molecule at −196 °C [30]. The pore-size distributions were computed by applying the Barrett–Joyner–Halenda (BJH) method [31].

2.2.2. Morphology study. Before the observations of SEM, the samples were plated with a thin layer of gold and observed with a LEO1530 VP SEM. Generally, HNTs could be dispersed in strong polar solvents such as water and *N*,*N*-dimethyl formamide (DMF). BBT could also be dissolved in DMF. Therefore DMF was selected to disperse the samples for TEM. 1 wt% HNTs DMF dispersion or HNTs/BBT (10/1, weight ratio) DMF dispersion were prepared by ultrasonic treatment. Then the solutions were dipped into the perforated carbon film on Cu grids and the dried samples were observed in a Philips Tecnai 12 TEM.

2.2.3. In situ FTIR. The experiment was performed with the MAGNA-IR760 (Nicolet Co, USA) equipped a heating furnace with the heating rate 5 °C min^{-1} from room temperature to 240 °C. The HNTs/BBT complex was pelleted with potassium bromide. Thirty-two consecutive scans were taken and their average was stored. Spectra were taken from 4000 to 400 cm^{-1}. The resolution of the wavenumber is 4 cm^{-1}.

2.2.4. Differential scanning calorimetry (DSC). DSC heating scanning of BBT and the HNTs/BBT complex were measured on a TA Q20 using nitrogen as purging gas. The samples were

heated to 250 °C at a ramping rate of 5 °C min^{-1}. The melting points of the samples were determined as the temperature at the maximum endothermic peak. All the DSC experiments were repeated for reliable data of the melting points.

2.3. Preparation of PP/HNTs/BBT nanocomposites

A two-screw extruder was used to prepare the PP/HNTs/BBT nanocomposites. The temperature setting of the extruder from the hopper to the die was 180/190/195/200/200/190 °C, and the screw speed was 100 rpm. The pelletized granules were dried for 5 h under 80 °C and then injection molded under a temperature of 200 °C.

2.4. Characterization of the PP/HNTs/BBT nanocomposites

2.4.1. Scanning electron microscopy (SEM). The impact-fractured surface of the composites was plated with a thin layer of gold before the observations. The SEM observations were done using a LEO1530 VP SEM.

2.4.2. Transmission electron microscopy (TEM). Ultrathin sections (200 nm) of the samples were cut using an ultramicrotome (EM ULTRACUT UC, Leica) and the sections were supported by a perforated carbon film on Cu grids. TEM analysis of the nanocomposites was carried out with a Philips Tecnai 12 TEM with an attached x-ray energy-dispersive spectrometer (X-EDS) was used to obtain elemental compositions of the fibrils.

2.4.3. Differential scanning calorimetry (DSC). DSC data was measured by a NETZSCH DSC204 F1 using nitrogen as purging gas. The samples were heated to 200 °C at a ramping rate of 20 °C min^{-1}. The sample was kept at 200 °C for 5 min to eliminate the thermal history before it is cooled down to 40 °C at a rate of 10 °C min^{-1}. The endothermic and exothermic flows were recorded as a function of temperature. All the DSC experiments were repeated for reliable data of the enthalpies and the endothermic peak temperatures.

2.4.4. Mechanical properties determinations. Specimens for the tensile, flexural and impact testing were injection molded and measured according to ISO 527: 1993, ISO 178: 1993 and ISO 180: 1993, respectively. Zwick/Roell Z010, Instron 4465 and Zwick pendulum 5113.300 were used to perform the tensile, flexural and impact testing, respectively.

2.4.5. Polarized optical microscopy (POM). The morphologies of the crystallites of the composites were recorded with an Olympus BX41 POM. The sample was prepared by scraping the melt of the samples between two slides and cooling in air at 20 °C.

3. Results and discussion

3.1. Characterization of interaction between HNTs and BBT

Surface area and pore structure analysis is an effective method for characterizing surface characteristics of nanoparticles.

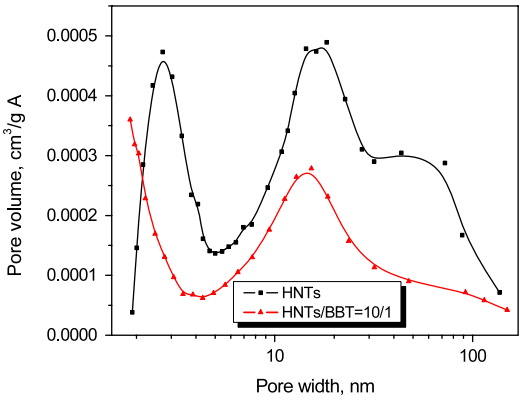

Figure 1. BJH pore-size distribution of HNTs and the HNTs/BBT complex.

Figure 1 shows the BJH pore-size distribution of HNTs and the HNTs/BBT complex. For HNTs, the three peaks of the pore volume versus pore width curve around 3, 17 and 50 nm are attributed to surface defects, the lumens of the nanotubes and pores among the tubes, respectively. For the HNTs/BBT complex, however, only the peak around 17 nm, characterizing the lumen's structure, survived. The disappearing of the 3 nm characterizing the surface defects may be explained by the adsorption of the BBT molecule onto the HNTs. As Solomon *et al* reported, the crystal edges of clay, in another way the surface defects, were the bare aluminum atoms, which could accept foreign electrons [32]. Because the HNTs are multi-wall nanotubes, the crystal edges may also be located in the interlayer of the HNTs. Therefore the electron-accepting sites may also be located in the interlayer. The adsorption of BBT on HNTs is observed by TEM, as shown in figure 2. The pristine HNTs have very clean and smooth walls. For the HNTs/BBT complex, however, the walls of the HNTs are much rougher and small particles of BBT are found to be located on the surface and lumens of the HNTs. The disappearing of the peak around 50 nm may be due to the pores among the tubes being occupied by BBT after the complexation. This is also shown by the SEM photos in figure 3. As shown, in the HNTs/BBT complex, BBT acts as 'glue' for the HNTs and connects the nanotubes. As a result, the BET surface area of the HNTs/BBT complex decreases from 50.45 m^2 g^{-1} for pristine HNTs to 25.82 m^2 g^{-1} for the complex. Strong interaction also affects the melting temperature of BBT. As shown in figure 4, the melting point determined by the DSC method is increased from 184.2 °C for BBT to 186.6 °C for the complex. The DSC recorded melting point is lower than in the commercial data as the latter is determined by the capillary tube method. The smaller peak in DSC curves is due to the impurities of the industrial grade BBT. This is consistent with the DSC result of the complex of CNTs and gamma-cyclodextrin (γ-CD), in which the strong interaction between CNTs and γ-CD was also suggested [33].

To verify the electron transfer mechanism between HNTs and BBT, *in situ* FTIR measurement of the HNTs/BBT complex was performed. Due to the structure of the electron transfer complex, it may be short-lived and not

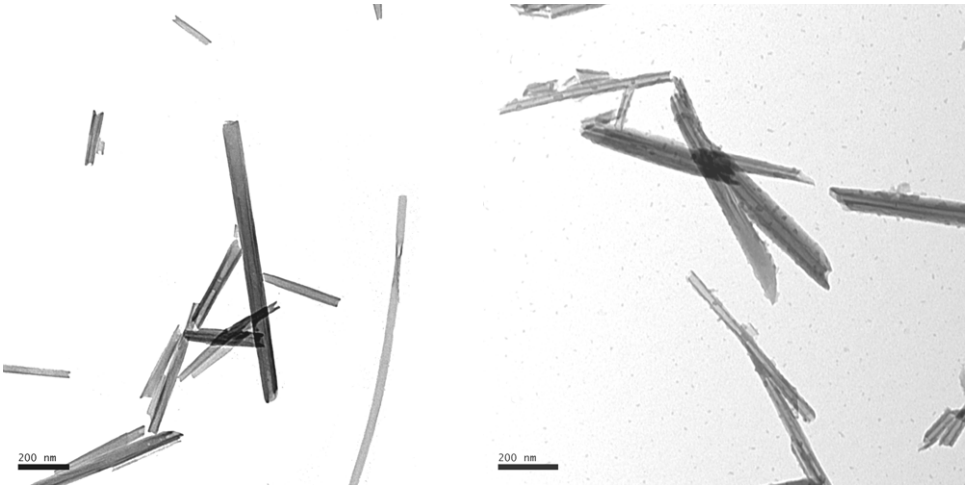

(a) (b)

Figure 2. TEM photos of HNTs (a) and the HNTs/BBT complex (10/1) (b).

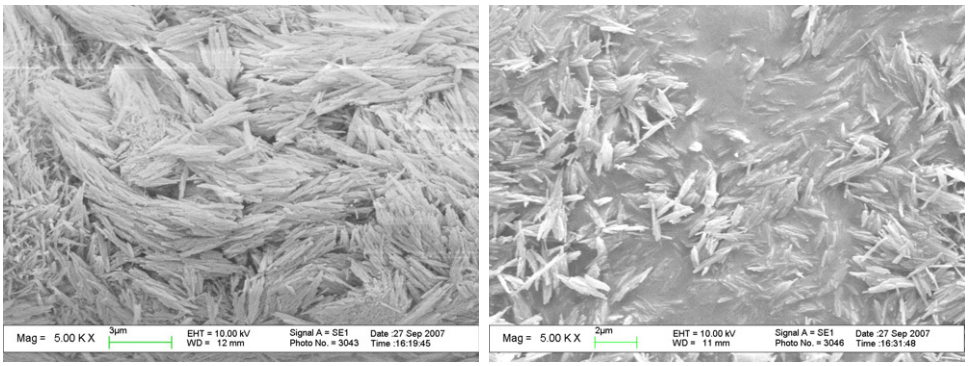

(a) (b)

Figure 3. SEM photos of HNTs (a) and the HNTs/BBT complex (10/1) (b).

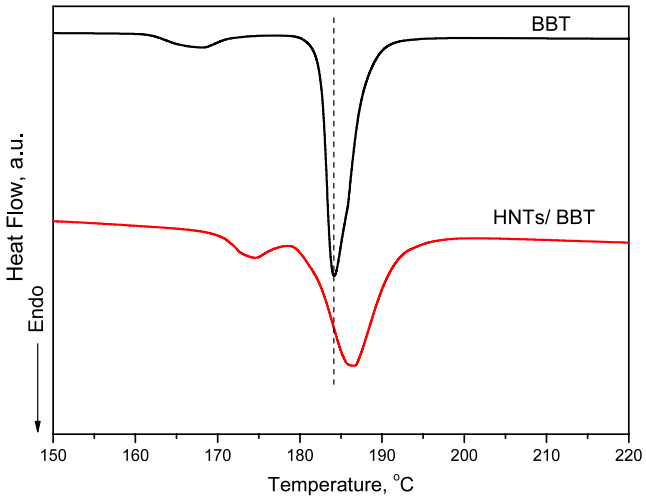

Figure 4. Heating scan curves of BBT and the HNTs/BBT complex by the DSC method.

easily monitored using the static FTIR technique. Therefore, as Gary Hastings suggested [34], time-resolved step-scan FTIR difference spectroscopy with a heating procedure for the study of the electron transfer process was used. The evolution of the FTIR spectrum of the HNTs/BBT complex during heating is presented in figure 5. The peak around 1580 cm^{-1} is assigned to the C=C bond of the benzene ring attaching atom with lone electron pairs [35]. For BBT, the N and O atoms in the benzoxazolyl group are neighbors to the benzene ring. A strong peak at 1580 cm^{-1} of the complex is observed at the relatively low temperature. With the measurement temperature, the intensity of the peak is decreased and blueshifted consistently, and eventually the peak is almost indiscernible at 200 °C. This can be explained by the fact that the N and O atoms in the BBT have lone electron pairs and have the capability of donating electrons. Under heating, the electron transfer from BBT to the HNTs takes place. Therefore, the BBT molecule plays the role of the electron donor while the aluminum atom or Fe^{3+} of the HNTs act as the electron acceptors in the present system.

In order to further investigate the structural change of BBT after the interaction with the HNTs, the model compound consisting of BBT and HNTs was prepared and treated at 200 °C for 20 min. Visual color change is a direct method for examining the structural variation of organic molecules. Figure 6 shows the photos of the BBT/HNTs complex and

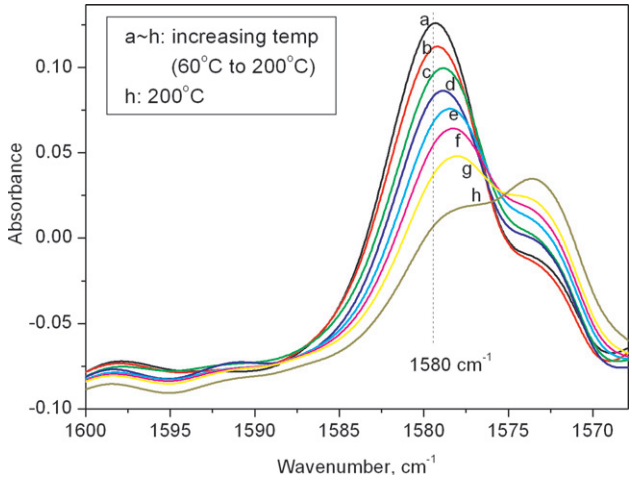

Figure 5. *In situ* FTIR spectra of the HNTs/BBT complex during heating.

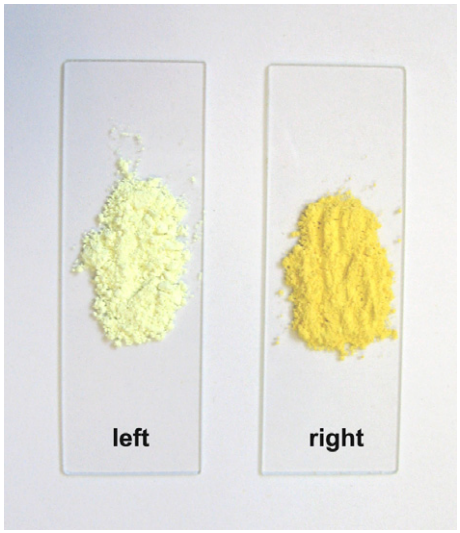

Figure 6. Photos of the HNTs/BBT complex (left) and the heat-treated HNTs/BBT complex (right).

the heated BBT/HNTs complex. The color change of the HNTs/BBT before and after the heat treatment is obvious. The color of the complex changed from light yellow to dark yellow after the heat treatment, indicating interactions take place between BBT and the HNTs during heating. Actually, color changes induced by electron transfer interactions have been widely reported [36–39].

3.2. Morphology of PP/HNTs/BBT nanocomposites

Figure 7 shows the SEM photos for the PP/HNTs/BBT nanocomposites. It can be seen that HNTs are uniformly dispersed in the PP matrix. Comparing with other nanofillers, the HNTs aggregate can be more easily separated under shearing in the polymer matrix due to the following reasons. Geometrically, the rod-like HNTs are more easily dispersed than the spherical particles. Chemically, HNTs are recognized as with low hydroxyl density in the HNTs surface compared with fumed silica and other layered silicates such as montmorillonite. Therefore, the interactions induced by hydrogen bonding among the tubes are relatively weaker. Apart from the nanotubes, as shown in figures 7(b) and (c), some ribbon-like or wire-like phase (fibrils) is observed in the PP/HNTs/BBT nanocomposites. With the increasing BBT content, more fibrils are obtained and fibrils tend to become longer and more continuous. As HNTs could not be aligned into such continuous fibrils, their formation is attributed to the organization of BBT molecules. Under the extrusion condition, BBT melts and interacts with HNTs to form the HNTs/BBT complex. The complex may be effectively oriented with shearing as BBT molecules and HNTs both have rod-like geometry and could be reorganized into aligned structures. Due to the strong interactions between BBT and HNTs, the aligned structures are continuously connected and composite fibrils consisting of BBT and HNTs are the result. Noticeably, as shown in figures 7(d) and (e), BBT itself could not be organized into fibrils in the absence of HNTs, indicating the critical role of HNTs for the formation of the fibrils. This process is depicted in scheme 1. The inset photo in scheme 1 is the SEM photo of the longitudinal side of the extrudate of the PP/HNTs/BBT composite. Clearly, the fibrils formed orient along the extrusion direction, indicating the critical role of melt shearing in the formation of the fibrils.

This interesting morphology of PP/HNTs/BBT nanocomposites was also verified by TEM. Figure 8 shows the TEM photos of the PP/HNTs/BBT nanocomposites. The fibrillar phase of BBT exists only in the nanocomposites with higher BBT content (10 phr). This may be attributed to the fact that the formed fibrillar phase of BBT may be destroyed upon re-heating. In the sample preparation process for the TEM observation, the samples were re-heated to 200 °C and compression molded to a thin film by static stress. The fibrils in the nanocomposites with lower BBT content may not survive under heating as the fibrils of BBT in the nanocomposites with lower BBT content are much less compared with those with higher BBT content. As a consequence, the fibrillar phase of BBT is only found in the nanocomposites with higher BBT content (10 phr).

3.3. Energy spectrum analysis of the fibrils in the nanocomposites

The chemical composition of the fibrils was examined by x-ray EDS elemental analysis of the TEM sample. Table 1 summarized the relative elemental content in regions 1 (fibril-rich region) and 2 (HNTs-rich region) in figure 8(c). The elements Cu and Ta come from the Cu girds used as the sample supporter in TEM observation. The main chemical composition of region 1 in figure 8(c) is C, O and S. Little Al and Si come from the HNTs. As sulfur is the characteristic element of BBT and no sulfur is found in the HNTs, the fibrillar phase in the nanocomposites consists of largely BBT and little HNTs. The element composition of region 2 is very different from region 1. No sulfur is detected in region 2, which indicates BBT does not exist in region 2. The chemical composition in region 2 is mainly of HNTs and PP matrix.

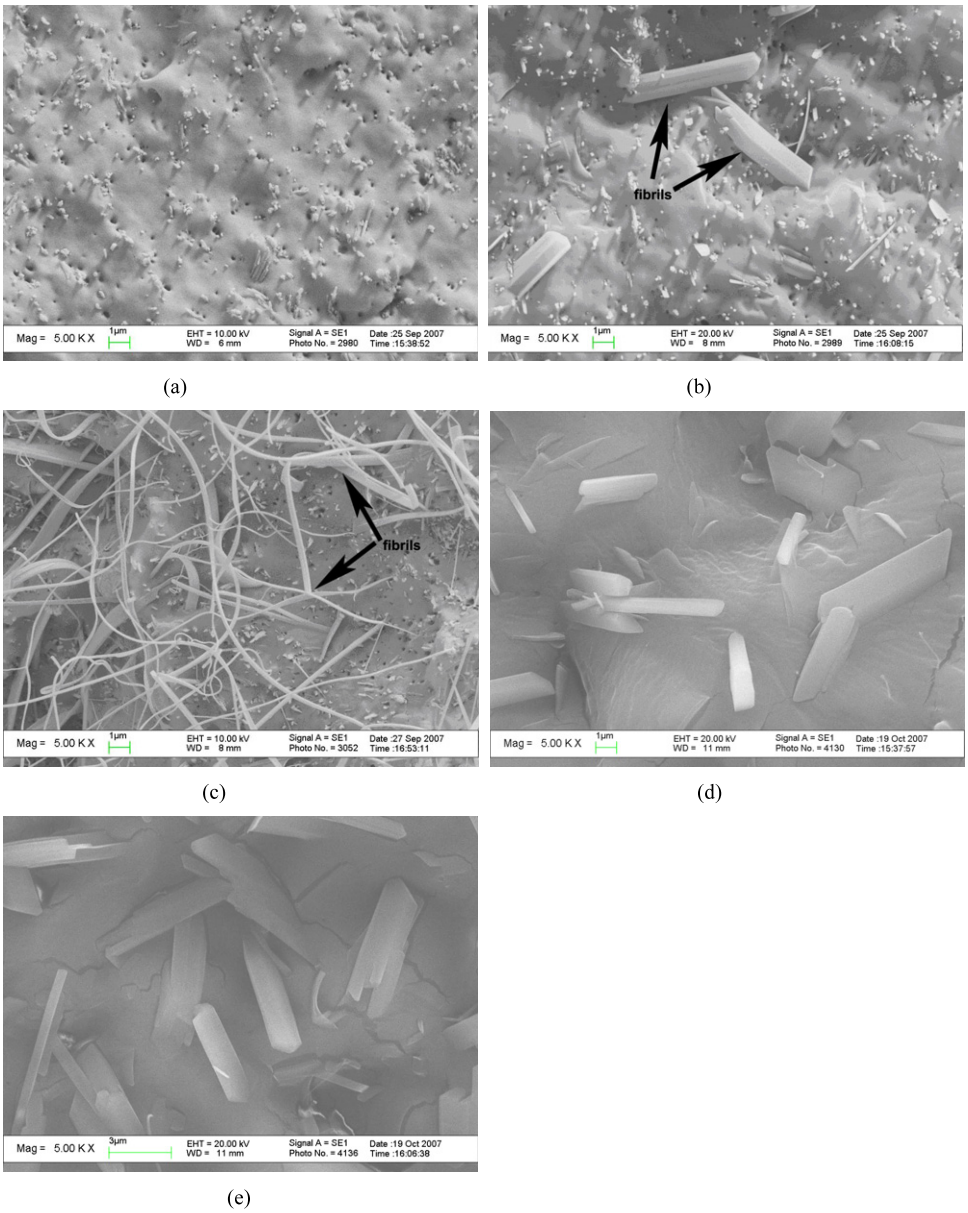

Figure 7. SEM photos of the impact fractured surface of the PP/HNTs/BBT nanocomposites: (a) PP/30 phr HNTs; (b) PP/30 phr HNTs/3 phr BBT; (c) PP/30 phr HNTs/10 phr BBT; (d) PP/3 phr BBT; (e) PP/10 phr BBT.

Another evidence for chemical composition of the fibrils is the difference in oxygen content in the two regions. As shown in table 1, the oxygen content in region 2 is much higher than that in region 1. This can be explained by the fact that the oxygen content of BBT is much lower than that of the HNTs. In short, the results of energy spectrum analysis indicate that the fibrils are composed mainly of BBT molecules.

3.4. Crystallization behavior of PP/HNTs/BBT nanocomposites

The crystallization property of PP/HNTs/BBT nanocomposites was examined by the DSC method. Table 2 summarizes the data from the DSC curves. Although the crystallization temperature of the nanocomposite is almost independent of the BBT content, the crystallinity of PP in the nanocomposite is

Table 1. X-ray EDS spectra data of regions 1 and 2 in figure 8(c).

Region	Element	Weight per cent (%)	Atom per cent (%)
1	C	8.66	31.80
	O	1.49	4.10
	Al	0.71	1.16
	Si	0.73	1.14
	S	0.54	0.75
	Cu	88.04	61.09
	Total	100.00	
2	C	9.66	34.27
	O	1.75	4.65
	Al	1.03	1.63
	Si	0.94	1.42
	Cu	86.51	58.01
	Ta	0.11	0.03
	Total	100.00	

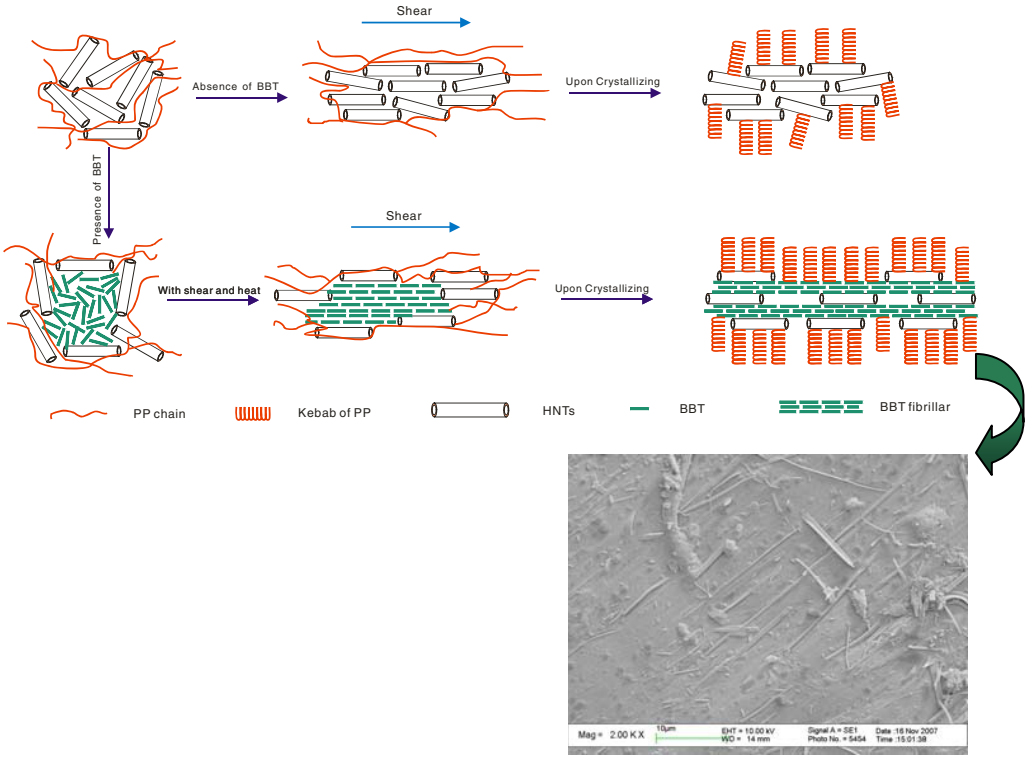

Scheme 1. Formation and structure of the fibrils in the PP/HNTs/BBT nanocomposites. (Inset SEM photo: longitudinal view of the extrudate of the PP/HNTs/BBT(100/30/10).)

Table 2. Data of PP/HNTs/BBT nanocomposites from DSC measurement and the calculated crystallinity.

Samples	Heat enthalpy (J g^{-1})	Crystallinity (%)	Crystallizing peak temperature (°C)
Neat PP	97.36	46.5	109.2
PP/HNTs (100/30)	76.80	47.8	120.3
PP/HNTs/BBT (100/30/0.5)	86.30	53.9	121.4
PP/HNTs/BBT (100/30/1)	96.39	60.4	122.2
PP/HNTs/BBT (100/30/3)	99.19	63.1	121.1
PP/HNTs/BBT (100/30/10)	93.64	62.7	122.5

significantly increased by incorporating BBT. The crystallinity of the PP in the composite was calculated according to the equation

$$\text{Crystallinity (\%)} = \frac{\Delta H_f}{\Delta H_f^0 \times C}$$

where ΔH_f and ΔH_f^0 are the endothermic enthalpies of the sample and that of the 100% crystallized PP (209 J g^{-1} [40]), respectively. C is the PP weight percentage in the composite. It can be seen from table 2 that HNTs cannot significantly increase the crystallinity of PP. The crystallinity of the composites with 30 phr HNTs is only 1.3% higher than that of the neat PP. However, incorporating BBT into the PP/HNTs nanocomposites leads to remarkably increased crystallinity of PP. For example, incorporation of 0.5 phr and 3 phr BBT leads to a 7.4% and 16.6% increase in crystallinity, respectively. The unprecedented results may originate from the fact that the crystal PP may grow along the fibrils, as shown in scheme 1. The nucleating ability of different fibers such as carbon fiber, glass fiber and polymeric fibers for the crystallization of PP was reported extensively [41, 42]. For example, the PP transcrystallites on polyethylene terephthalate (PET) fibrils were observed in *in situ* microfibrillar PET/PP blends during the extrusion process [43]. Recently, Fu *et al* reported a hybrid shish kebab structure, with PE crystal lamellae periodically decorated on the surface of SiO_2–MgO–CaO whiskers (SMCW) and aligned approximately perpendicular to the long axis of the SMCW. The effect of shear in the processing could be considered as adding more active nucleation sites on the whisker surface, thus weakening the requirement of lattice matching, resulting in a growth of so-called soft epitaxy on much larger diameters of whisker [44]. In the present systems, the mesogenic structure of BBT acts as the nucleating points. The growth of PP spherulites on the mesogenic structure of BBT may be hindered as the fibrils provide continuous alignment of densely and closely packed nuclei [45, 46]. The continuous alignment of the closely packed nuclei, however, leads to more growth of the PP shish kebab on the fibrils, resulting in the coexistence of incomplete spherulites and shish kebab. This is evidenced by the POM observations, as shown in figure 9. It is clear that, after the incorporation of BBT, the spherulites are less complete compared with those in the PP/HNTs nanocomposites. In addition, fibrillar crystallites are observed in the BBT-containing samples, indicating coexistence of incomplete spherulites and shish kebab. As a result, this particular morphology brings substantially higher crystallinity, possibly due to more dense packing of PP crystallites.

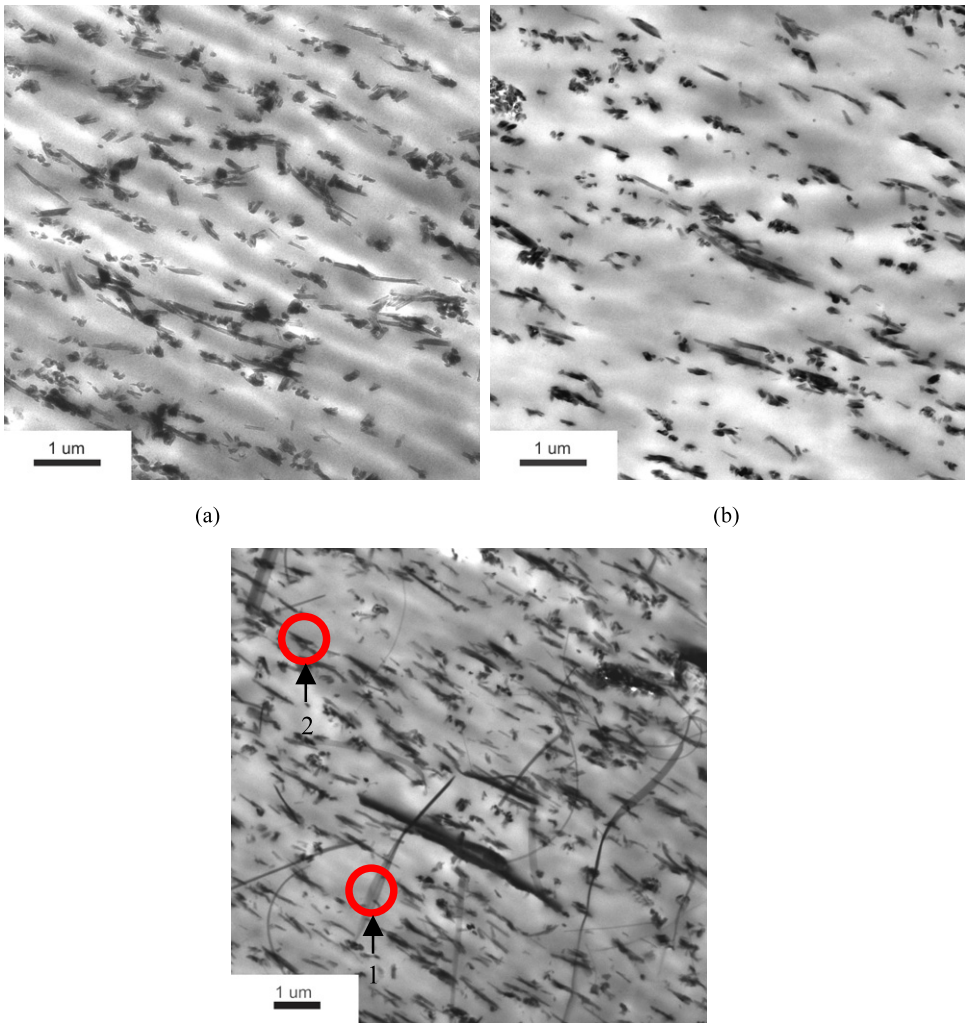

Figure 8. TEM photos of PP/HNTs/BBT nanocomposites: (a) PP/30 phr HNTs; (b) PP/30 phr HNTs/3 phr BBT; (c) PP/30 phr HNTs/10 phr BBT.

Table 3. Mechanical properties of PP/HNTs/BBT nanocomposites (data in parentheses indicates the standard deviations).

Samples	Tensile strength (MPa)	Flexural strength (MPa)	Flexural modulus (MPa)	Impact strength (kJ m^{-2})
Neat PP	33.2 (0.5)	41.8 (1.0)	1244 (26)	6.65 (0.66)
PP/HNTs(100/30)	31.9 (0.1)	46.1 (0.9)	1779 (65)	4.85 (0.19)
PP/BBT(100/3)	33.8 (0.5)	43.3 (0.9)	1276 (41)	5.86 (0.25)
PP/BBT(100/10)	31.9 (0.2)	44.8 (1.1)	1347 (52)	4.95 (0.19)
PP/HNTs/BBT(100/30/0.5)	35.8 (0.2)	55.1 (0.5)	2290 (52)	4.65 (0.70)
PP/HNTs/BBT(100/30/1)	36.5 (0.5)	56.6 (0.9)	2449 (30)	3.91 (0.13)
PP/HNTs/BBT(100/30/3)	37.7 (0.1)	58.2 (0.2)	2509 (18)	3.73 (0.07)
PP/HNTs/BBT(100/30/10)	38.8 (0.2)	61.4 (0.5)	2830 (94)	3.13 (0.26)

3.5. Mechanical properties of PP/HNTs/BBT nanocomposites

Crystallinity of polymers is one of the important factors in determining the mechanical properties of composites. The higher crystallinity of the polymer usually brings the high modulus and strength of the polymer composites. The mechanical properties of the PP/HNTs/BBT nanocomposites are shown in table 3. The tensile strength, flexural strength and flexural modulus of the PP/HNTs/BBT nanocomposites are substantially increased by BBT, although the impact strength of the nanocomposites with BBT is decreased. The tensile strength, flexural strength and flexural modulus of the nanocomposites with 10 phr BBT are 22%, 33% and 59% higher than those of the PP/HNTs, respectively. The mechanical properties of the composites only with BBT, however, show little increase in mechanical properties

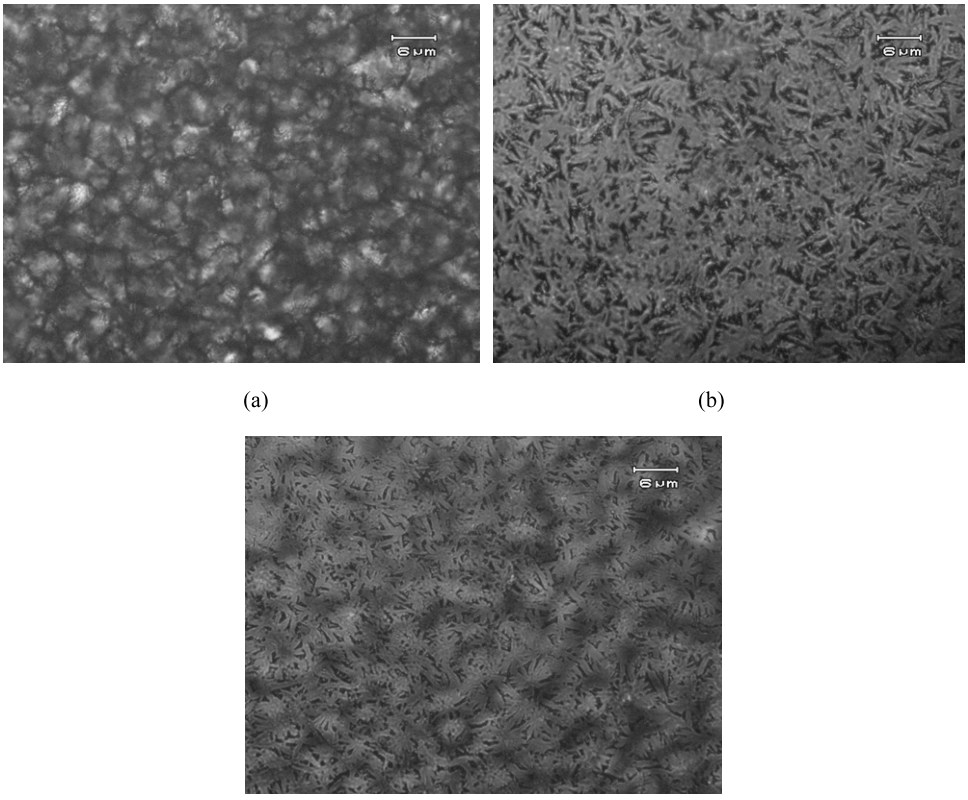

Figure 9. POM photos of PP/HNTs/BBT nanocomposites: (a) PP/30 phr HNTs; (b) PP/30 phr HNTs/3 phr BBT; (c) PP/30 phr HNTs/10 phr BBT.

compared with those of the neat PP. As a consequence, the positive reinforcing effect of BBT for PP/HNTs nanocomposites is attributed to the formation of BBT fibrils in the nanocomposites. The formation of the fibrils leads to increased crystallinity of the matrix and consequently the tensile and flexural properties of the nanocomposites are increased substantially. The decreased impact strength of the BBT-incorporated nanocomposites may be due to the transcrystalline layer of PP on the BBT fibril surface, which possesses high rigidity and lower deformability [47, 48].

4. Conclusions

A conjugated molecule, 2,5-bis(2-benzoxazolyl) thiophene (BBT), capable of donating electrons, was selected as the interfacial modifier for polypropylene (PP)/halloysite nanotubes (HNTs) nanocomposites. The electron transfer interactions between the HNTs and BBT were confirmed. The unusual morphology of the nanocomposite was observed. BBT was aligned into a fibril structure in the presence of HNTs under the processing of the nanocomposites. The formation mechanism of BBT fibrils was elucidated to be due to the strong interactions between BBT and HNTs and the melt shearing. The formation of the BBT fibrils led to much higher crystallinity compared with previously reported PP nanocomposites. The nanocomposites with BBT showed substantially increased tensile and flexural properties, which were attributed to the enhanced crystallinity of the nanocomposites. Although the surface chemistry and geometry of carbon nanotubes (CNTs) are quite different from those of HNTs, in our opinion, the idea of designing an interface via charge transfer may also be applicable to CNTs incorporating polymer composites.

Acknowledgment

We are grateful for the financial support by the National Natural Science Foundation of China with grant no. 50603005.

References

[1] Friedrich K, Fakirov S and Zhang Z 2005 *Polymer Composites: From Nano- to Macro-Scale* (Berlin: Springer)
[2] Hussain F, Hojjati M, Okamoto M and Gorga R E 2006 *J. Compos. Mater.* **40** 1511–75
[3] Kang S, Hong S I, Choe C R, Park M, Rim S and Kim J 2001 *Polymer* **42** 879–87
[4] Tsujii Y, Ohno K, Yamamoto S, Goto A and Fukuda T 2006 *Surface-Initiated Polymerization I* (*Book Series: Advances in Polymer Science* vol 197) pp 1–45
[5] Radhakrishnan B, Ranjan R and Brittain W J 2006 *Soft Matter* **2** 386–96
[6] Pukanszky B and Fekete E 1999 *Mineral Fillers in Thermoplastics I* (*Book Series: Advances in Polymer Science* vol 139) pp 109–53

[7] Bauer F, Glasel H J, Decker U, Ernst H, Freyer A, Hartmann E, Sauerland V and Mehnert R 2003 *Prog. Org. Coat.* **47** 147–53
[8] Ray S S and Okamoto M 2003 *Prog. Polym. Sci.* **28** 1539–641
[9] Manias E, Touny A, Wu L, Strawhecker K, Lu B and Chung T C 2001 *Chem. Mater.* **13** 3516–23
[10] Usuki A, Hasegawa N and Kato M 2005 *Adv. Polym. Sci.* **179** 135–95
[11] Wang Y, Chen F B and Wu K C 2004 *J. Appl. Polym. Sci.* **93** 100–12
[12] Ning N Y, Yin Q J, Luo F, Zhang Q, Du R N and Fu Q 2007 *Polymer* **48** 7374–84
[13] Du M L, Guo B C, Liu M X and Jia D M 2007 *Polym. J.* **39** 208–12
[14] Du M L, Guo B C and Jia D M 2006 *Eur. Polym. J.* **42** 1362–9
[15] Liu M X, Guo B C, Du M L, Cai X J and Jia D M 2007 *Nanotechnology* **18** 455703
[16] Singh B 1996 *Clays Clay Miner.* **44** 191–6
[17] Joussein E, Petit S, Churchman J, Theng B, Righi D and Delvaux B 2005 *Clay Miner.* **40** 383–426
[18] Du M L 2007 *PhD Dissertation* South China University of Technology
[19] Solomon D H and Rosser M J 1965 *J. Appl. Polym. Sci.* **9** 1261–71
[20] Solomon D H and Swift J D 1967 *J. Polym. Sci.* A **11** 2567–75
[21] Talapatra S, Saha S K, Chakravarti S K and Guhaniyogi S C 1983 *Polym. Bull.* **10** 21–7
[22] Talapatra S, Guhaniyogi S C and Chakravarti S K 1985 *J. Macromol. Sci. Chem.* **A22** 1611–21
[23] Weissmahr K W, Haderlein S B, Schwarzenbach R P, Hany R and Nuesch R 1997 *Environ. Sci. Technol.* **31** 240–7
[24] Solomon D H 1968 *Clays Clay Miner.* **16** 31–9
[25] Carr R M and Chih H 1971 *Clay Miner.* **9** 153–66
[26] Theng B K G 1974 *The Chemistry of Clay-Organic Reactions* (London: Hilger)
[27] Adachi C, Tsutsui T and Saito S 1990 *Appl. Phys. Lett.* **56** 799–801
[28] Wu L H, Wang Y C and Hsu C S 2000 *Liq. Cryst.* **27** 1503–13
[29] Shchukin D G, Sukhorukov G B, Price R R and Lvov Y M 2005 *Small* **1** 510–513
[30] Brunauer S, Emmett P H and Teller E 1938 *J. Am. Chem. Soc.* **60** 309–19
[31] Barrett E P, Joyner L G and Halenda P P 1951 *J. Am. Chem. Soc.* **73** 373–80
[32] Solomon D H, Loft B C and Swift J D 1968 *Clay Miner.* **7** 389–97
[33] Chambers G, Carroll C, Farrell G F, Dalton A B, McNamara M, In Het Panhuis M and Byrne H J 2003 *Nano Lett.* **3** 843–6
[34] Golbeck J H 2006 *Photosystem I: The Light-Driven Plastocyanin: Ferredoxin Oxidoreductase* (Berlin: Springer) chapter 20
[35] *The Sadtler Handbook of Infrared Spectra* 2004 Bio-Rad Laboratories Inc., Informatics Division
[36] Nagamura T, Sakaguchi H, Ito T and Muta S 1994 *Mol. Cryst. Liq. Cryst. Sci. Technol.* A **247** 39–48
[37] Nagamura T, Ichihara T and Kawai H 1996 *J. Phys. Chem.* **100** 9370–6
[38] Morikawa M, Kimizuka N, Yoshihara M and Endo T 2002 *Chem. Eur. J.* **8** 5580–4
[39] Friggeri A, Gronwald O, van Bommel K J C, Kjeld J C, Shinkai S and Reinhoudt D N 2002 *J. Am. Chem. Soc.* **124** 10754–8
[40] Brandrup J and Immergut E H 1989 *Polymer Handbook* 3rd edn (New York: Wiley) chapter V
[41] Wang C and Liu C R 1999 *Polymer* **40** 289–98
[42] Chou S and Chen S H 2000 *Polym. Polym. Compos.* **8** 267–79
[43] Li Z M, Li L B, Shen K Z, Yang W, Huang R and Yang M B 2004 *Macromol. Rapid Commun.* **25** 553–8
[44] Ning N Y, Luo F, Pan B F, Zhang Q, Wang K and Fu Q 2007 *Macromolecules* **40** 8533–6
[45] Schonhorn H 1991 *Macromolecules* **24** 3569–77
[46] Billon N, Henaff V and Haudin J M 2002 *J. Appl. Polym. Sci.* **86** 725–33
[47] Riley A M, Paynter C D, McGenity P M and Adams J M 1990 *Plast. Rubber. Process. Appl.* **14** 85–93
[48] Folkes M J and Hardwick S T 1987 *J. Mater. Sci. Lett.* **6** 656–8